ResearchGate

See discussions, stats, and author profiles for this publication at: https://www.researchgate.net/publication/222067669

Experimental constraints on high pressure melting in subducted crust

Article *in* Earth and Planetary Science Letters · May 2001

DOI: 10.1016/S0012-821X(01)00321-1

CITATIONS
248

READS
95

2 authors:

Joerg Hermann
Universität Bern
266 PUBLICATIONS **14,795** CITATIONS

SEE PROFILE

David Headley Green
University of Tasmania
268 PUBLICATIONS **28,498** CITATIONS

SEE PROFILE

Some of the authors of this publication are also working on these related projects:

Influence of C + H +O on melting in the Earth's Upper Mantle, View project

Nanogranitoids and crustal melting View project

All content following this page was uploaded by Joerg Hermann on 26 June 2018.

The user has requested enhancement of the downloaded file.

ELSEVIER

Earth and Planetary Science Letters 188 (2001) 149–168

EPSL

www.elsevier.com/locate/epsl

Experimental constraints on high pressure melting in subducted crust

Jörg Hermann *, David H. Green

Research School of Earth Sciences, The Australian National University, Mills Road, Acton, Canberra, ACT 0200, Australia

Received 11 October 2000; received in revised form 13 February 2001; accepted 22 March 2001

Abstract

Synthesis piston-cylinder experiments were carried out from 2.0 to 4.5 GPa and 850 to 1150°C in order to determine phase and melting relations in a model composition for subducted crust (K_2O–CaO–MgO–Al_2O_3-SiO_2–H_2O). As subduction zone magmas are enriched in H_2O and large ion lithophile elements (LILE), this study concentrates on the stability of phases that host these elements. Biotite and phengite were found to be the stable phases able to transport H_2O and LILE to mantle depths. At pressures below 3.0 GPa biotite is stable to higher temperatures than phengite and melting related to biotite breakdown occurs at about 950°C. At higher pressure, only phengite melting occurs along the reaction phengite+clinopyroxene+coesite → garnet+kyanite+melt+K-feldspar, which has a positive slope to 1050°C, 4.5 GPa. Biotite reacts to phengite under subsolidus conditions with the conservation of LILE and H_2O stored in the rock. The stability of phengite to high pressures and temperatures prevents liberation of LILE and H_2O by 'fluid absent' melting in subduction zones with a normal thermal gradient. It is suggested that these elements are probably released by melting in the presence of fluids, which derive from dehydration of the mafic or ultra-mafic layer of the slab. The experiments demonstrate that melts produced by mica melting or by addition of small amounts of H_2O at lower temperatures are granitic in composition and display an increase of K_2O with increasing temperature. Determination of trace element partitioning between melt and residue indicates that the heavy rare earth elements will be incorporated in garnet and strongly enriched in the residue whereas the LILE preferentially enter the melt even if there is phengite in the residue. The light rare earth elements (LREE) are not significantly enriched in the granitic melts because of small amounts of LREE-rich allanite in the residue. Such hydrous granitic melts could participate in the metasomatism of the mantle wedge and might be partly responsible for the characteristic trace element patterns of subduction zone magmas. © 2001 Elsevier Science B.V. All rights reserved.

Keywords: experimental studies; partial melting; subduction; phengite; trace elements; crust

1. Introduction

Subduction zone magmas are characterized by depletion of high field strength elements (HFSE) and enrichment of K, Rb, Sr, Ba and Cs (large ion lithophile elements, LILE) with respect to MORB [1–3]. Based on correlation between the composition of sediment inputs and magma outputs in subduction zones, it has been suggested that the elevated LILE composition derives from a 'sediment component' which is transferred from

* Corresponding author. Tel.: +61-2-6125-8842; Fax: +61-2-6125-5989; E-mail: joerg.hermann@anu.edu.au

0012-821X/01/$ – see front matter © 2001 Elsevier Science B.V. All rights reserved.
PII: S0012-821X(01)00321-1

the subducting oceanic crust to the mantle [4]. There has been a long-running debate as to whether these elements are transferred by melts [5] or fluids [6,7]. However, the finding of the 'second critical point' in silicate+H_2O systems at high pressures, beyond which separate fluid and melt cannot exist [8,9], blurs this distinction. Instead we need to know which minerals incorporate these elements, under which conditions these minerals break down, what are the reaction products and what is the partitioning of elements between solid and melt/fluid phases.

Studies on high pressure rocks from paleo-subduction zones demonstrate that phengite is the most important K phase in high pressure rocks with crustal protoliths [10–13]. Trace element studies on natural phengite from eclogites revealed that most of the LILE are hosted in phen-

Table 1
Composition of the starting materials and of those melts, which have been analyzed for trace elements

Sample	P1	P2	*C-825*	*UHP50*	C-983	C-896	C-905	C-907	UHP60
T (°C)			950	1000	950	1000	1000	1150	1080
P (GPa)			3.5	4.52	3.0	3.5	3.0	3.5	4.2
Major elements (wt%):									
SiO_2	61.5	59.5	66.45	63.57	66.67	65.92	66.17	66.88	65.98
Al_2O_3	21	21	12.34	12.36	12.72	12.33	12.39	13.61	13.40
MgO	8	8	0.71	0.41	0.54	0.57	0.71	1.00	0.53
CaO	6	6	1.77	1.21	1.48	2.52	2.00	4.06	1.57
K_2O	3	3	8.05	8.87	8.49	6.96	7.17	6.50	10.03
Na_2O	0.2	2.5	0.22	0.39	0.18	0.17	0.10	0.21	0.26
Sum			89.54	86.80	90.07	88.47	88.54	92.25	91.76
Calculated or estimated values:									
H_2O			10	9	7	7	6	5	8
% melt			15	20	35	40	40	40	35
Al*			1	0.99	1.04	0.99	1.07	0.92	0.95
Kfs			50	58	53	44	45	40	62
Plag			11	10	9	15	12	23	11
Qtz			37	31	36	40	40	38	28
Trace elements (ppm):									
Rb	357		946	606	580	728	658	808	929
Sr	226		861	541	304	425	399	537	562
Y	251		25	7.5	5.8	15	11	46	6.6
Zr	271		276	222	127	203	236	457	230
Ba	299		873	595	422	583	521	730	744
La	235		123	171	151	359	360	592	534
Ce	283		151	209	175	416	415	673	584
Nd	121		60	79	48	126	139	234	129
Sm	107		45	34	12	38	54	105	29
Eu	129		53	30	12	39	72	103	27
Gd	100		25	13	6	14	14	44	10
Yb	136		7.2	1.9	1.7	3.7	3.4	15	1.6

The 0.2% of Na in the starting material P1 originates from contamination of the ingredients. The trace element content of the starting material represents an average of 14 ICP-MS analyses. Runs in italics contain melts buffered in all components. The H_2O content of the melts can be estimated on the basis of three constraints. (1) A maximum content of H_2O is given by the difference from 100% to the totals of the oxide components of microprobe analyses. (2) When the melt is the only phase containing H_2O and potassium, the H_2O content can be calculated from the K_2O/H_2O ratio of the starting material (Fig. 6a). (3) H_2O content can be estimated from mass balance based on approximate volume and measured composition of the different phases. For run in italics, approach 3, for the other runs approach 2 was mainly used to estimate the water content. Estimated relative errors for the H_2O content of melts are $\sim$20%. Vol% of melt is estimated from run product analyses and from the K_2O content of the melts. Excess Al* is calculated as molar Al/(Na+K+2*Ca). Calculated amounts of K-feldspar, plagioclase and quartz are given in oxygen%. Typical relative 1σ errors are 1–2% for SiO_2, 2–4% for Al_2O_3, 10–25% for MgO, 3–5% for CaO and K_2O and 10–15% for trace elements.

gite and thus this hydrous mineral is crucial for LILE transfer from subducted crust to the mantle [10,14]. There is a number of experimental studies on the stability of phengite in K-MORB, greywacke and sedimentary compositions which all point to a stability of phengite to great depth [15–17].

This study has sought to complement the existing experiments by conducting experiments in the K_2O–CaO–MgO–Al_2O_3-SiO_2–H_2O (KCMASH) synthetic system. This is the simplest system in which it is possible to generate the high pressure phases phengite, coesite, garnet, clinopyroxene and kyanite. These minerals occur in different proportions in all rock types of subducted crust. The advantage of using a synthetic system is to have a strong control on phase relations and reactions. We report a petrogenetic grid for the melting of biotite and phengite in KCMASH and evaluate the pressure (P) and temperature (T) dependence of fully buffered melt compositions. Experiments were doped with trace elements in order to determine rock/melt partitioning. On the basis of the experimental data, possible mechanisms for LILE release during subduction are discussed and the consequences of partial melting for the properties of subducted crustal material are emphasized.

2. Starting material

The oxide proportions of the starting material (Table 1) were chosen in order to obtain saturation of kyanite and quartz/coesite, and similar amounts of the high pressure phases garnet, clinopyroxene and phengite. A combination of key trace elements was added at a 100–350 ppm level (Table 1). The starting material P1 was prepared using the 'sol–gel procedure' [18] in order to homogenize the trace elements. MgO, K-carbonate, Al-nitrate and the trace elements as carbonates or nitrates were dissolved in HNO_3 and the resulting acid solution was slowly evaporated until it started to crystallize. The brine was then diluted with water and ethanol and silica was added as tetra-orthosilicate. Gel formation was triggered by addition of ammonia. A part of the dried gel was fused to a glass at 1400°C for 20 min to increase the density of the starting material. In experiments labeled P1, water was added using a microsyringe. Two additional mixes were also made in which H_2O was added as hydrous phases, to more precisely control the amount of free H_2O in the experiments. P1b consists of a sintered oxide mix with addition of natural Mg-phengite and Mg-talc and has the same major element composition as P1. $Al(OH)_3$ is the H_2O source in the oxide mix P1c which contains 10 wt% of H_2O and identical oxide proportions as P1. The desired amount of H_2O in various experiments conducted was obtained by blending P1c and P1 mixes in different proportions. P2a contains 2.5 wt% Na_2O replacing 2.5 wt% of SiO_2, but with no other change to P1. H_2O was added to P2a as natural Mg-phengite. The amount of H_2O added in most experiments was 2.5 wt%, which exceeds H_2O contents able to be stored in micas in the chosen bulk composition by about 1.2 wt%. The experiments are thus slightly oversaturated in H_2O to enhance reaction rates at the low experimental temperatures, but not so H_2O-rich as to risk losing the K phases by solubility of components in the melt at significantly lower temperatures than their breakdown reaction.

3. Experimental and analytical techniques

Synthesis experiments were run in an end-loaded 1.27 cm piston-cylinder apparatus at the Research School of Earth Sciences (ANU). 15–20 mg of sample was loaded in a Pt capsule (outside diameter = 2.3 mm) sealed by arc welding. The capsule was maintained below 100°C during welding by immersion in water-soaked tissue paper. A low friction assembly was used consisting of teflon foil, NaCl and pyrex sleeves, a graphite heater and sintered MgO inserts, in which the Pt capsule was embedded. Pressure calibration against the quartz/coesite transition demonstrated that there is no need for a friction correction with this assembly. Thus, pressure in the experiments is measured by load on the piston and is accurate to ± 0.1 GPa. Runs at $P = 4.0$ GPa were conducted with a highly polished piston and pusher in a 200

ton end-load press or in a 500 ton end-load press (labeled as UHP runs) using a shorter piston (2.2 cm instead of 3.8 cm). In order to maintain enough piston travel on the 500 ton press to reach high pressures, a longer steel plug was used and an internal pressure of about 1.0 GPa was obtained by applying the confined pressure at about 2 mm of piston travel. Hardened steel plugs were used in both types of experiments. Pressure was adjusted several times during the first 24 h of runs to compensate pressure drop due to the release of internal friction. Temperature was controlled using type B thermocouples ($Pt_{94}Rh_6/Pt_{70}Rh_{30}$) and is accurate to ±10°C. The sample was quenched at the end of the run by terminating the power to the furnace. Capsules were recovered, cut in half with a diamond saw and mounted in epoxy.

Phase relations were analyzed in polished mounts by back-scattered electron (BSE) images on a JEOL 6400 scanning electron microscope (SEM) (Electron Microscopy Unit, ANU). The phase compositions were determined by EDS, using an acceleration voltage of 15 kV and a beam current of 1 nA. The K_2O content of glasses analyzed using focussed 1 μm spots were found to be systematically low compared to 6 μm per 10 μm area scans. A correction procedure accounting for the decrease of K_2O in time (Fig. 1) was established in order to determine the K_2O content of small melt pools, where scan analyses could not be applied. The K_2O concentration of melts, analyzed with area scans, reaches a plateau during the 110 s of counting for an electron probe EDS analysis and represents the best possible estimate for the K_2O content of the melt. The K_2O concentration decreases as a function of time when melts are analyzed with a 1 μm spot due to the instability of K_2O in glass under an electron beam. The K_2O content obtained at the end of a spot analyses is typically 15–20% lower than the one determined by scan analysis. The scan value can be satisfactory approached by extrapolating the spot-time series to a '0-time'.

Melt trace element analysis was performed on the laser ablation-inductively coupled plasma mass spectrometry (ICP-MS) at the RSES (ANU) [19]. Ablation was done with a pulsed 193 nm ArF excimer laser with an energy flux of about 20 J/cm^2 at a repetition rate of 5 Hz and pit size of 23 μm. A mixed Ar–He stream was used to transport the aerosol into the Fisons PQ2+ICP-MS where 22 masses were analyzed. Detection limits were of the order of 0.05 ppm for most rare earth elements (REE). The trace element composition of the starting glass material was measured in every batch of analyses as a secondary standard.

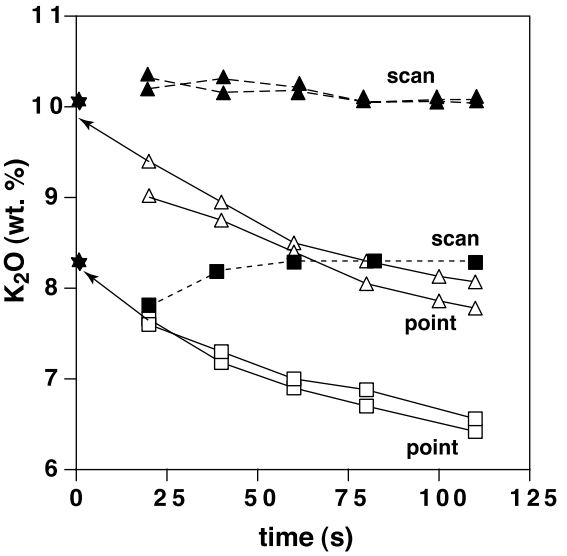

Fig. 1. Time series for scan analyses (filled symbols) and spot analyses (open symbols) of K_2O in two different hydrous granitic glasses. The '0-time' value of spot analyses is very close to the value obtained from scan analyses (black stars). This procedure permits analysis of small melt pools in the experimental run products.

4. Experimental results

The experimental conditions and synthesized phase assemblages are presented in Table 2 and plotted in Fig. 2. The minerals form euhedral to subeuhedral grains with 5–20 μm in diameter (Fig. 3) and can easily be determined with the SEM–EDS system. The shape of coexisting minerals suggest that textural equilibrium was reached in the experiments (Fig. 3). Clinopyroxene, kyanite and quartz/coesite are the most common phases and occur nearly over the whole *P–T*

range investigated. Kyanite disappears at the lowest pressure, highest temperature conditions investigated, most probably because of the large amount of garnet and melt present. Garnet is generally isometric and poikiloblastic with irregular coesite inclusions and appears at the high temperature/high pressure part of the grid (Fig. 2). The amount of garnet with respect to clinopyroxene increases with increasing pressure and temperature and at 1080°C and 4.2 GPa, there is no clinopyroxene left. Biotite is stable up to 900°C and 3.0 GPa, whereas phengite was found at lower temperatures below 3.0 GPa. Above 3.0 GPa, phengite is stable to higher temperatures (up to 1000°C) and its upper pressure stability has not been reached within the investigated P–T space. Orthopyroxene appears in a small field between the biotite and garnet stability fields. K-Feldspar was found in three runs. Run C-910 and C-1191 contained no excess H_2O, whereas C-870 most probably experienced water loss during welding, which could explain the presence of K-feldspar (see below). Allanite was found as accessory mineral in nearly all runs doped with trace elements. It was possible to quench the melt in all experiments and no quench phases were observed.

5. Mineral composition

Representative mineral compositions of the experimental run products are provided in the

Table 2
Experimental run conditions and products. Phases in bold are present in the run products in the range of 10–50 vol%, others at 1–10%

Run No.	Mix	P (GPa)	T (°C)	h	wt% H_2O	Phases
C-810	P1	3.5	900	187	2.6	**Cpx, Cs, Phe, Grt, Ky, Melt**, Opx, *All*
C-825	P1	3.5	950	304	2.5	**Cpx, Cs, Phe, Grt, Ky, Melt**, *All*
C-879	P1	3.5	850	155	5.3	**Cpx, Cs, Phe, Opx, Ky, Melt**, *All*
C-870	P1	3.5	1050	186	3.1?	**Cpx, Cs, Grt, Melt**, Kfs, Ky, *All*
C-896	P1	3.5	1000	99	2.9	**Cpx, Cs, Grt, Ky, Melt**, *All*
C-905	P1	3.0	1000	95	2.7	**Cpx, Cs, Grt, Ky, Melt**, Opx
C-907	P1	3.5	1150	65	2.4	**Cpx, Cs, Grt, Ky, Melt**
C-910	P2a	3.5	970	119	1.1	**Cpx, Cs, Grt, Melt**, Kfs, Phe, Ky
C-929	P1b	2.0	900	140	2.2	**Cpx, Qtz, Bt, Melt**, Opx, Ky, (Grt)
C-934	P1b	2.5	1000	189	2.2	**Cpx, Qtz, Grt, Melt**, (Bt)
C-936	P1	3.0	900	240	3.5	**Cpx, Cs, Grt, Ky, Melt, Opx,** Phe, Bt, *All*
C-939	P1b	2.5	1050	171	2.2	**Cpx, Qtz, Grt, Melt**
C-940	P1b	2.0	1000	163	2.2	**Cpx, Qtz, Grt, Melt**, Opx
C-942	P1c	2.5	840	80	4.5	**Cpx, Qtz, Ky, Bt, Melt**, All,
UHP50	P1c	4.52	1000	72	2.5	**Cpx, Cs, Phe, Grt, Ky, Melt**, *All*
C-982	P1c	2.5	950	165	2.5	**Cpx, Qtz, Ky, Opx, Grt, Melt,** *All*
C-983	P1c	3.0	950	168	2.5	**Cpx, Cs, Ky, Grt, Melt,** Opx, *All*
UHP56	P1c	4.05	1000	72	2.5	**Cpx, Cs, Phe, Grt, Ky**, Melt, *All*
C-988	P1c	2.0	850	266	2.5	**Cpx, Qtz, Bt, Ky,** Zo/All, Melt
C-989	P1c	3.0	850	264	2.5	**Cpx, Cs, Phe, Bt, Ky**, Melt, *All*
UHP60	P1c	4.2	1080	72	2.5	**Cs, Grt, Ky, Melt**
C-1080	P1c	2.5	900	187	2.5	**Cpx, Qtz, Bt, Ky**, Melt?, *All*
C-1115	P1c	4.5	1050	73	2.7	**Cs, Grt, Ky, Melt**, Cpx, *All*
C-1187	P1c	3.0	940	98	1.3	**Cpx, Cs, Phe, Bt, Ky**
C-1191	P1c	2.5	1000	96	1.3	**Cpx, Qtz, Ky, Grt, Melt**, Kfs

Italics refer to accessory minerals ($<1\%$). Phases in parentheses are stabilized by traces of Ti and Fe which occur in the natural phengite and talc used in the P1b starting material and are not considered as stable phases in the KCMASH system. Abbreviations (also valid for the following figures and tables): P = pressure, T = temperature, h = time in hours, Cs = coesite, Qtz = quartz, Phe = phengite, Cpx = clinopyroxene, Opx = orthopyroxene, Grt = garnet, Ky = kyanite, M = melt, Bt = biotite, Kfs = K-feldspar, Zo = Zoisite, All = Allanite.

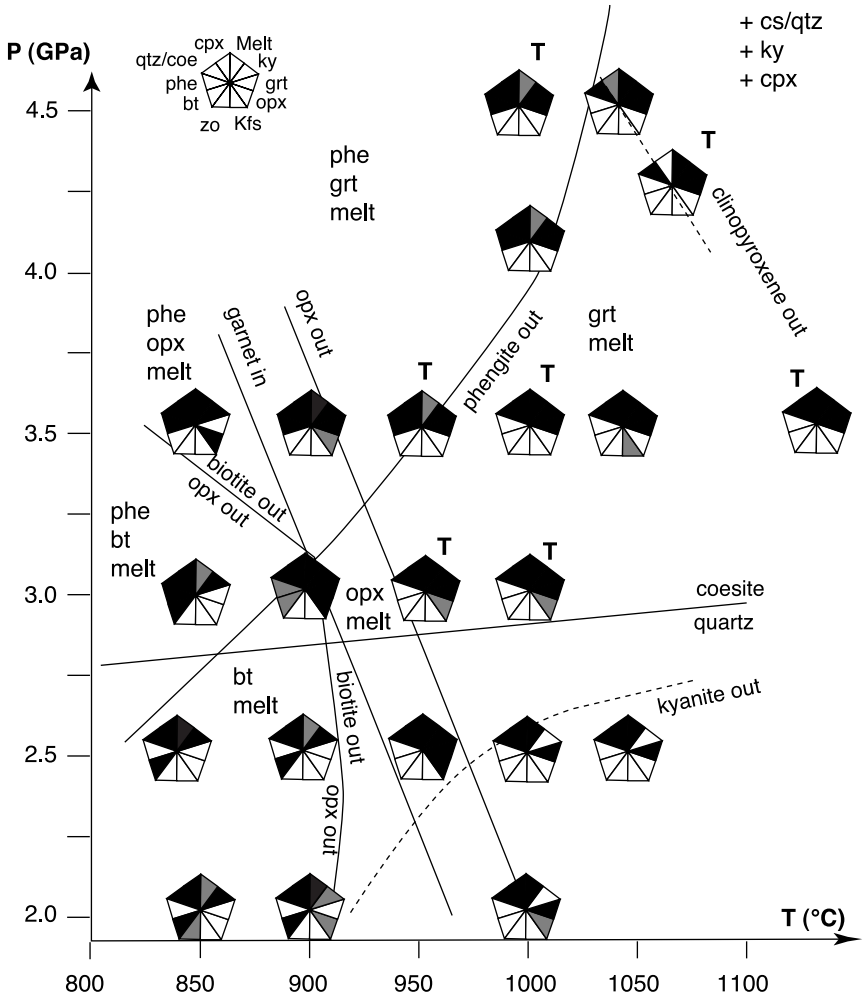

Fig. 2. Results of the experimental runs and the stability of the different phases. Major phases are shown in black and minor phases are given in gray. Melt coexists with phengite because of small amounts of excess H_2O in the experiments (Fig. 6). The main parageneses in the different P–T regions are indicated. The dashed lines indicate limits of a phase due to complete consumption during melt formation and cannot be used to constrain univariant reactions. In experiments labeled with (T) trace element composition of the melt could be analyzed (see Table 1). The coesite/quartz transition is taken from Mirwald and Massone [48].

EPSL Online Background Dataset[1]. Mineral compositions are generally homogeneous through the whole section of the capsule and display little zoning. An exception is clinopyroxene, which often displays Al-rich cores and occasionally whole grains with Al contents well above average. Nevertheless, clinopyroxene rims and grains belonging to the major compositional population display a regular increase of the $CaAl_2SiO_6$ component with temperature (Fig. 4a) but no significant pressure effect. The Ca content of garnet increases with increasing pressure at a fixed temperature (Fig. 4b) and to a lesser extent with increasing temperature at a fixed pressure. These trends are in agreement with calculated trends using the Berman thermodynamic dataset [20]. The

[1] http://www.elsevier.nl/locate/epsl, mirror site: http://www.elsevier.com/locate.epsl

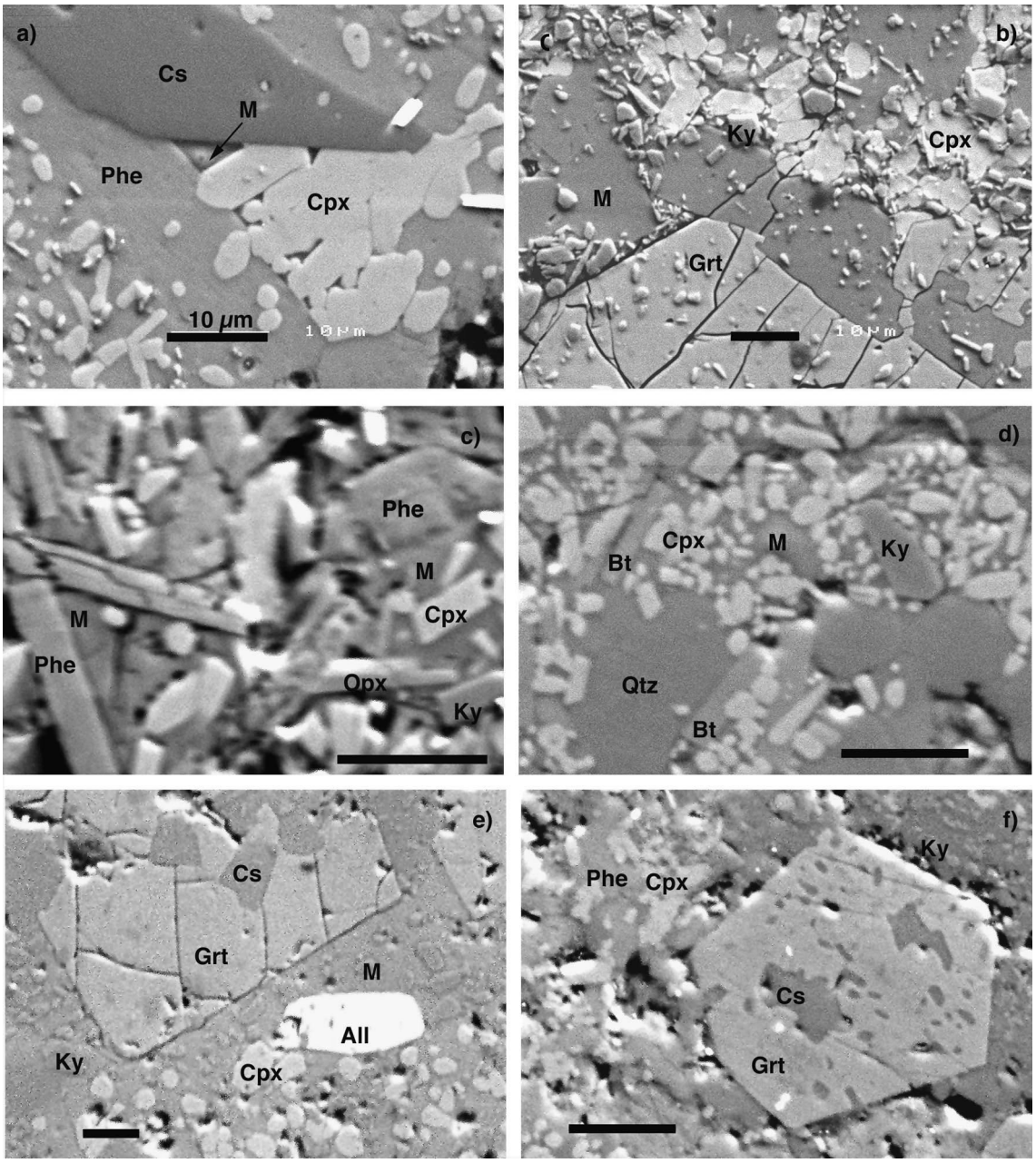

Fig. 3. Back-scattered electron images of run products. Scale bar is 10 μm. (a) Melt patch at a triple junction between clinopyroxene, phengite and coesite. Run C-825 (950°C, 3.5 GPa). (b) Larger melt patches contain small kyanite inclusions and are often associated with garnet. Run C-825 (950°C, 3.5 GPa). (c) Melting is fluxed by excess H_2O in run C-879 at 850°C, 3.5 GPa. Textures indicate equilibrium between melt and phengite. (d) At 2.0 GPa, 900°C (run C-929) biotite has a higher thermal stability than phengite and coexists with melt. (e) Allanite coexists with melt in run C-896 (1000°C, 3.5 GPa). (f) Typical subsolidus paragenesis of subducted crust with garnet, phengite, clinopyroxene, coesite and kyanite (UHP56, 4.05 GPa, 1000°C). For abbreviations see Table 2.

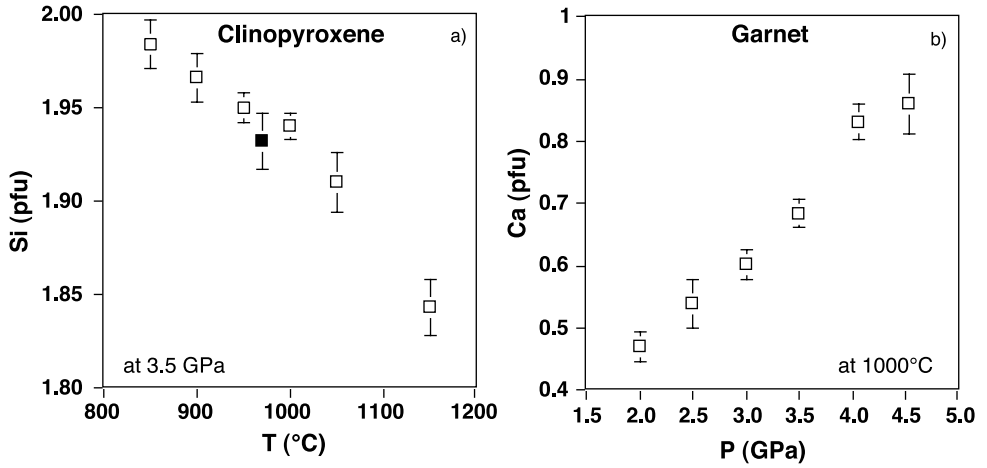

Fig. 4. The regular trends of mineral compositions with temperature and pressure indicate that the experiments attained chemical equilibrium. Bars refer to 1σ errors of multiple analyses. (a) The Si content of clinopyroxene decreases with increasing temperature indicating an increasing amount of $CaAl_2SiO_6$ component. Note that the Na-bearing experiment (filled symbol) also plots perfectly on the trend. (b) The Ca content of garnet increases with increasing pressure.

regular trends of mineral compositions with changing pressure and temperature and the agreement with trends based on thermodynamic data provide further indication that the experiments reached equilibrium.

The Si content of phengite reaches the highest value of 3.45 pfu at 1000°C, 4.52 GPa. The very similar Si contents of 3.37 at 950°C, 3.5 GPa and 3.38 at 1000°C, 4.05 GPa indicate that Si-isopleths in phengite, which coexists with garnet, kyanite and coesite, have a positive slope, in agreement with other studies [21]. The Si content of biotite increases with pressure from 2.9 pfu at 2.0 GPa to 3.05 at 3.0 GPa. The accessory mineral allanite contains several wt% of La_2O_3 and Ce_2O_3 and up to 6 wt% of MgO at the expense of Al_2O_3 in order to compensate the incorporation of trivalent cations on the Ca site.

Table 3
Analyzed major element melt compositions (see Table 1 for explanations)

Sample	*C-870*	*C-879*	*C-910*	*C-929*	*C-936*	*C-942*	*UHP56*	*C-988*	*C-810*	*C-1191*	C-934	C-939	C-940	C-982	C-1115
T (°C)	1050	850	970	900	900	840	1000	850	900	1000	1000	1050	1000	950	1050
P (GPa)	3.5	3.5	3.5	2.0	3.0	2.5	4.05	2.0	3.5	2.5	2.5	2.5	2.0	2.5	4.45
Major elements (wt%):															
SiO_2	67.74	66.36	67.14	66.49	66.28	66.10	65.56	66.44	67.07	67.78	67.31	66.91	66.87	68.80	64.12
Al_2O_3	13.85	11.19	13.47	13.25	12.40	11.93	13.33	13.53	12.54	13.49	12.62	12.91	13.58	12.83	13.21
MgO	0.36	0.77	0.61	1.23	0.91	0.77	0.91	0.87	0.40	0.54	1.02	1.29	1.85	0.71	0.39
CaO	1.18	3.05	0.57	2.97	2.09	4.18	1.48	2.76	1.17	1.64	2.02	2.79	3.78	1.59	1.40
K_2O	9.78	4.07	8.08	4.99	6.73	2.97	9.50	5.74	6.38	9.05	7.42	5.31	4.85	8.10	10.42
Na_2O	0.12	0.15	1.59	0.14	0.19	0.35	0.17	0.27	0.25	0.21	0.17	0.19	0.12	0.18	0.31
Σ	93.03	85.59	91.46	89.06	88.59	86.30	90.95	89.62	87.82	92.72	90.55	89.39	91.05	92.21	89.84
Calculated or estimated values:															
H_2O	5	14	7	6	10	13	8	8	12	5	5	4	4	7	8
% melt	25	15	10	10	25	15	5	10	10	25	40	55	60	35	30
Al*	1.07	1.1	1.09	1.2	1.09	1.05	1.01	1.16	1.33	1.03	1.05	1.16	1.1	1.07	0.92
Kfs	59	26	50	31	42	19	59	36	40	55	46	33	30	49	66
Plag	7	18	18	17	13	26	9	17	9	10	12	16	20	10	10
Qtz	31	53	29	46	41	53	29	42	45	33	39	45	44	38	25

6. Melt composition

The analyzed melts all have granitic compositions (Tables 1 and 3) and possess very similar contents of SiO_2 and Al_2O_3 when normalized on an anhydrous composition (Fig. 5a). They also have very low mafic component contents with MgO generally below 1 wt% (Tables 1 and 3). These melts are only slightly peraluminous with the highest Al over Ca and total alkali ratio occurring at lower temperatures and lower amounts of partial melting (Fig. 5b). The estimated H_2O content of the melts decreases with increasing temperature (Tables 1 and 3) and does not exceed 15 wt%. This relatively low amount of dissolved H_2O characterizes the 'liquid phase' as hydrous melts (e.g. [8,9])

In experiments where melt coexists with another K phase, the melt is buffered in all components of the KCMASH system (Fig. 6) and its compo-

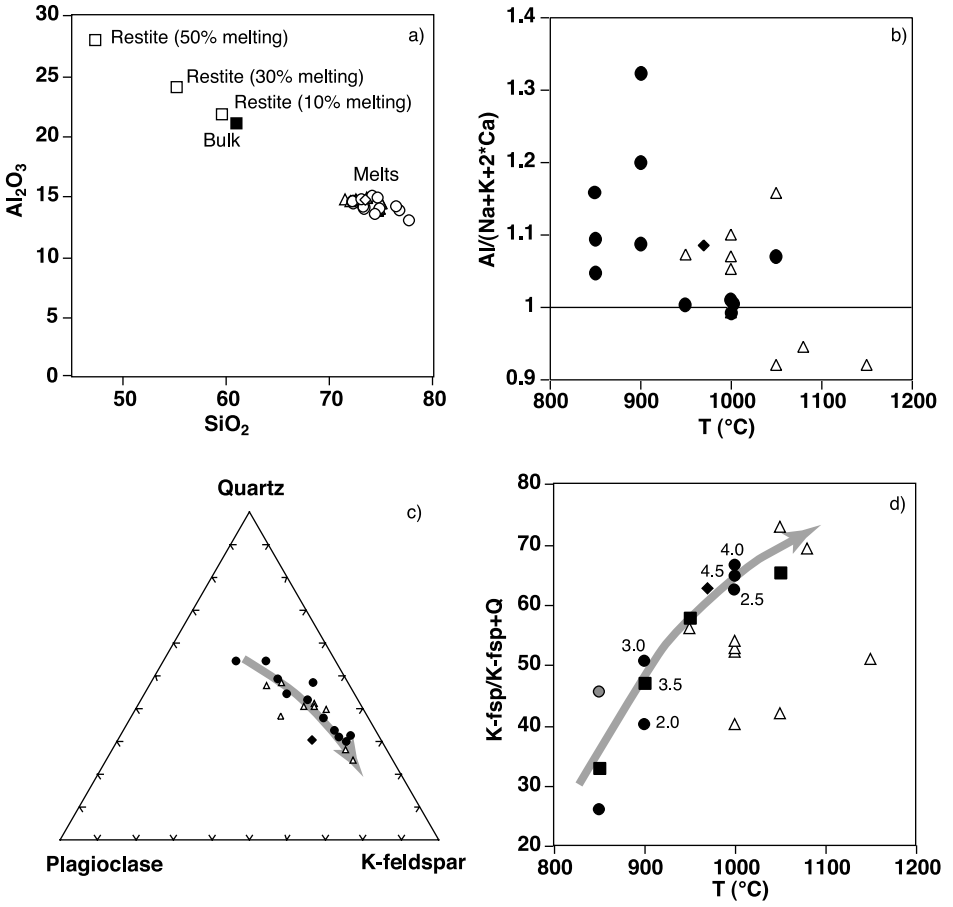

Fig. 5. Major element composition of the melts. (a) All melts have a 'granitic' (Na-free) composition and display only small variations when normalized on an anhydrous basis. The extraction of different amounts of granitic melt leads to a decrease of SiO_2 and increase of Al_2O_3 content in the residue, reflected by increasing garnet and kyanite in the restite. (b–d) Filled dots: completely buffered melts; open triangle: K is not buffered; diamond: completely buffered melt in the NKCMASH system. (b) The melts are only slightly peraluminous and only a small degree of partial melts occurring at lower temperatures contain excess Al. (c) Normative composition of the melts in terms of quartz, plagioclase and K-feldspar (given in oxygen%). The buffered melts describe a trend with decreasing plagioclase and increasing K-feldspar component. (d) This trend is mainly a function of temperature and does not display a systematic change with pressure (indicated in GPa for selected experiments). Filled squares display the trend in K-enrichment in the melt for a fixed pressure of 3.5 GPa. The deviation from the trend line indicates the degree of K-undersaturation of unbuffered partial melts (open triangles).

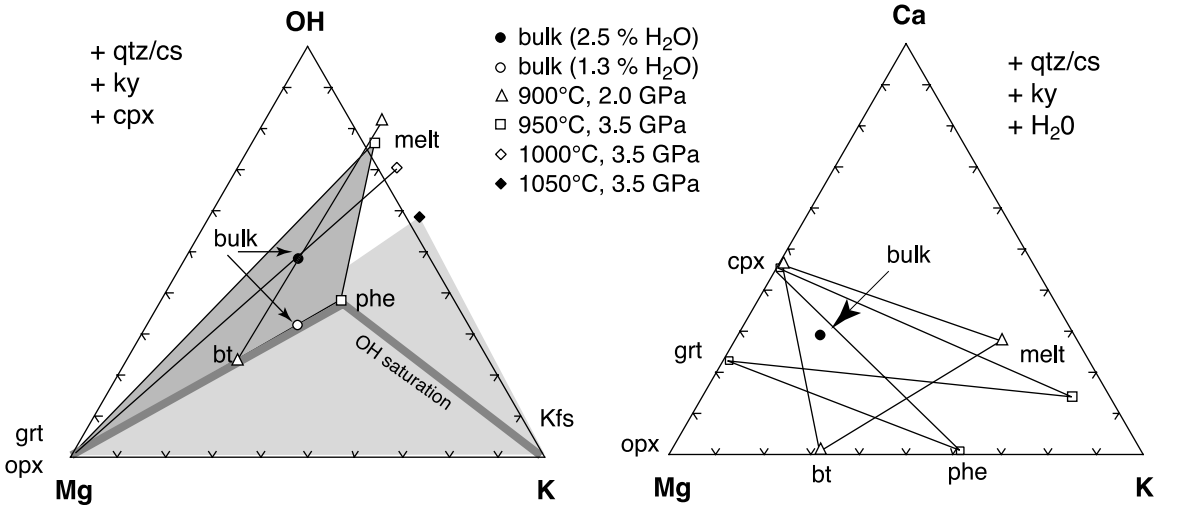

Fig. 6. Composition space for bulk rock and run products in molar proportions in different projections. (a) Almost all experiments contain clinopyroxene, kyanite and coesite/quartz permitting projection from these phases. Most of the starting compositions were slightly oversaturated in H_2O and therefore plot above the biotite–phengite tie-line. Run C-825 at 950°C, 3.5 GPa contains melt, phengite and garnet (dark gray triangle) and therefore the melt composition is buffered in all components. At 50°C higher temperatures (run C-896) phengite is not stable anymore. Because of the excess H_2O in the starting material there is no formation of K-feldspar and the K/OH ratio of the melt is determined by the starting material. If the starting composition is situated on the biotite–phengite tie-line (no excess H_2O), phengite breakdown produces garnet, melt and K-feldspar (light gray triangle) as in run C-870 at 1050°C, 3.5 GPa. (b) Because most experiments contain small amounts of excess H_2O, it is possible to use a second projection from kyanite, coesite/quartz and H_2O. The position of the bulk with respect to the phases determines which phases are completely consumed during the univariant reactions (Fig. 7, right).

sition may change as a function of pressure and temperature only. In the granite triangle, with plotted normative contents of plagioclase, K-feldspar and quartz, a clear compositional trend is visible with decreasing plagioclase and quartz contents and increasing K-feldspar content (Fig. 5c). The increase of normative K-feldspar with respect to quartz correlates with increasing temperature but does not show a correlation with pressure (Fig. 5d). Interestingly, one experiment performed in the NKCMASH system shows an increase of only about 10% of plagioclase component relative to the Na free system and still contains much more K-feldspar than plagioclase (black diamond in Fig. 5c, Table 3). This can be explained by the preferential incorporation of Na into the pyroxene relative to the melt in this run (partitioning Na cpx/melt $\sim$3.4). This melt composition plots precisely on the trend of K-feldspar enrichment with increasing temperature (Fig. 5d).

7. Phase relations

Because kyanite, quartz/coesite and clinopyroxene are stable over almost the whole investigated grid (Fig. 2) it is possible to project from these phases into the composition space (Fig. 6a). Clinopyroxene is completely consumed only at high pressures due to the continuous reaction:

$$\mathrm{Ky} + \mathrm{Cpx} + \mathrm{Melt}_1 \rightarrow \mathrm{Grt} + \mathrm{Cs} + \mathrm{Melt}_2 \qquad (1)$$

In the remaining P–T space there exist five solid phases and a melt in the phengite stability field and four solid phases and melt above phengite breakdown. This is consistent with the phase rule. In the KCMASH composition space, a divariant field should contain six phases including melt and a potassium phase. Above the breakdown of biotite and phengite, K-feldspar coexists with melt if no excess H_2O is added (Fig. 6a). With excess H_2O, melt is the only phase contain-

ing H_2O and potassium (Fig. 6a) and thus components (CMAS–KOH) and coexisting phases are reduced to five. The only exception to this general rule is the field with biotite and melt, which should contain six phases instead of five. However, as Fig. 6a demonstrates, there is a degeneration due to the chosen bulk composition being situated on a tie-line between biotite and melt. The fact that the phase rule is satisfied, provides an argument for the lack of metastable phases in these synthesis experiments.

Several reactions can be postulated in the KCMASH system on the basis of observed phases and their composition. The analysis of phase relations is presented in two steps. Firstly, the actual system with about 1.2 wt% of excess H_2O is discussed (Fig. 7, left) and secondly the results are extrapolated to a system without excess H_2O (Fig. 7, right). At 3.5 GPa, 950°C (run C-825; Table 2) melt patches occur at triple junctions between coesite, clinopyroxene and phengite (Fig. 3a). Large melt pools always coexist with garnet and kyanite (Fig. 3b). These textural relationships indicate that the phengite melting reaction is:

$$\mathrm{Phe} + \mathrm{Cpx} + \mathrm{Cs} \rightarrow \mathrm{Grt} + \mathrm{Ky} + \mathrm{Melt} \qquad (2a)$$

This is also consistent with the chemography (Fig. 6b), where the crossing of tie-lines phengite–clinopyroxene to garnet–melt indicate complete con-

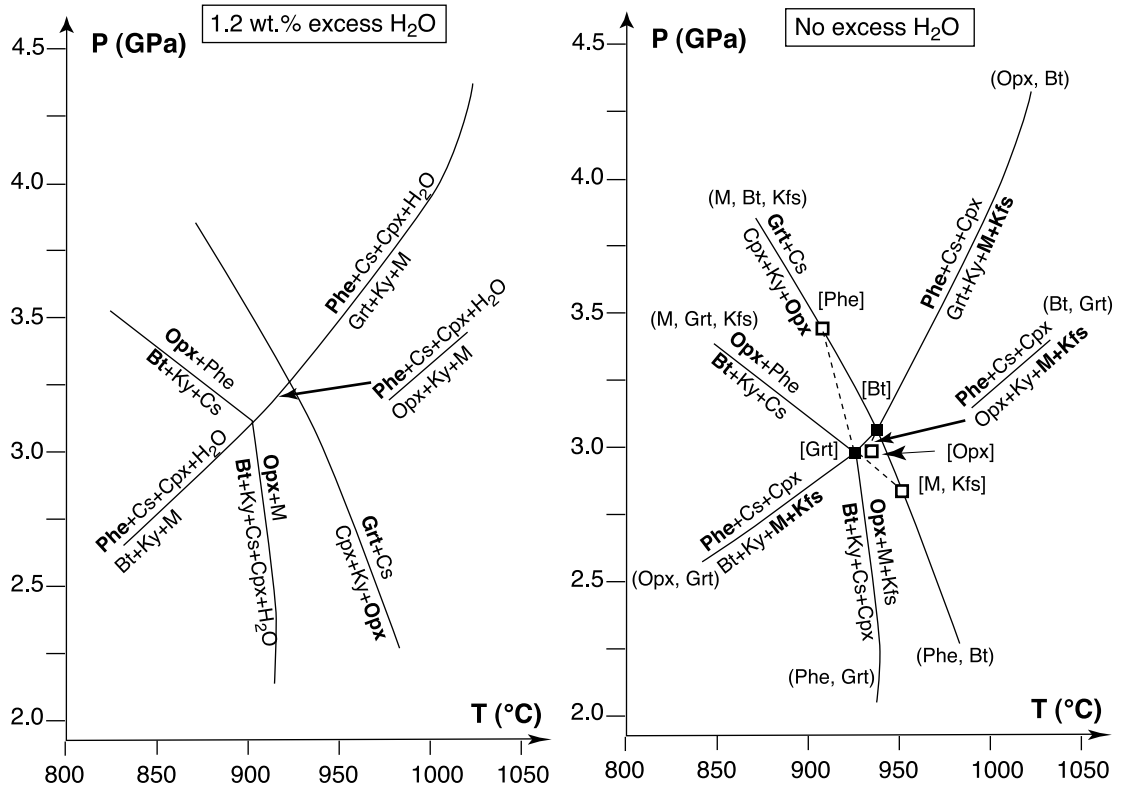

Fig. 7. Proposed reactions on the basis of textural observations, chemical composition of phases and their geometrical relations in the composition space (Fig. 6). Left: Limiting reactions in the system with small amounts of excess H_2O. Disappearing phases are given in bold. Right: Constructed *P–T* grid for 'fluid absent' melting. The phases in bold are consumed along the univariant reactions as a result of the chosen bulk composition (Fig. 6). Absent phases along univariant reactions are labeled with round brackets and absent phases at an invariant point are shown with square brackets. Metastable univariant reactions are shown with dashed lines. Stable invariant points are shown with a filled square and metastable invariant points are indicated with an open square.

sumption of phengite. Because there is a slight amount of excess H_2O, the reaction could be written as:

$$Phe + Cpx + Cs + H_2O \rightarrow Grt + Ky + Melt \quad (2b)$$

However, under these conditions and in the chosen bulk there is no distinction between vapor and melt and therefore the probably best representation of the reaction is:

$$Phe + Cpx + Cs + Melt_1 \rightarrow Grt + Ky + Melt_2 \quad (2c)$$

The melt volume continuously increases during this continuous reaction whereas the amount of phengite decreases. At a low water to phengite ratio, the maximum stability of phengite can be reached. Otherwise phengite is completely consumed before the breakdown reaction is reached. At pressures below 3.0 GPa, biotite has a higher thermal stability than phengite. Analogous to phengite, the disappearance of biotite is caused by the reaction:

$$Bt + Ky + Cpx + Cs + Melt_1 \rightarrow Opx + Melt_2 \quad (3)$$

The fluid absent reaction, which describes the transition from biotite to phengite in the KMASH subsystem, is unaffected by the amount of excess H_2O:

$$Bt + Ky + Cs \rightarrow Opx + Phe \quad (4)$$

Another fluid absent reaction describes the transition from orthopyroxene to garnet in the CMAS subsystem:

$$Cpx + Ky + Opx \rightarrow Grt + Cs \quad (5)$$

This reaction cannot be exactly located in *P–T* space because garnet and orthopyroxene occur together in a transition zone of about 50°C (Fig. 2).

A further effect of the excess H_2O is the general absence of K-feldspar as a run product. In experiments where no excess water was added, K-feldspar is formed during partial melting. This is in agreement with the chemical composition of fully buffered melts. At 3.5 GPa, the melts between 950 and 1050°C contain more OH with respect to K than phengite (Fig. 6a). Consequently, the breakdown of phengite will result in the formation of melt, K-feldspar and a Mg phase (Fig. 6a). On the basis of this information, a fully consistent grid for the 'fluid absent' system can be constructed using the experimental results, phase relations and Schreinemaker's rule (Fig. 7, right). The position of fluid absent reactions 4 and 5 are not affected and remain in the same position. The continuous reaction 2c consuming phengite translates in a discontinuous breakdown reaction:

$$Phe + Cpx + Cs \rightarrow Grt + Ky + Melt + Kfs \quad (6)$$

The transfer of structurally bound H_2O in hydrous phases to melt constrains 'fluid absent' melting (e.g. [22,23]). The position of this reaction must be situated at the same or higher temperatures than the investigated disappearance of phengite in the system with small amounts of excess water. At 3.5 GPa the reaction is thus at temperatures above 950°C. On the other hand, experiment C-910 contained no excess water and phengite breakdown was observed at 970°C. This experiment was conducted in a Na-bearing bulk system. Because Na partitions preferentially into clinopyroxene, which is on the reactant side of reaction 6, 970°C represent the upper temperature stability of phengite. This indicates that with addition of 1.2% of excess water and with 27 wt% of phengite in the starting material, phengite is not dissolved completely prior to its breakdown, which occurs at about 960°C at 3.5 GPa. At 3.0 GPa the shift of the reaction is higher because higher amounts of excess H_2O (2.4 wt%) have been used in experiment C-936. In fact, run C-1187 without excess H_2O still produced phengite and biotite at 940°C, indicating that phengite melting is at higher temperatures. From the orientation of reactions 4–6, the rest of the multisystem can be constructed (Fig. 7, right). It reveals that phen-

gite melting occurs below 3.0 GPa by the reaction:

$$\text{Phe} + \text{Cpx} + \text{Cs} \rightarrow \text{Bt} + \text{Ky} + \text{Melt} + \text{Kfs} \quad (7)$$

and biotite melting is related to reaction:

$$\text{Bt} + \text{Ky} + \text{Cpx} + \text{Cs} \rightarrow \text{Opx} + \text{Melt} + \text{Kfs} \quad (8)$$

The disadvantage of adding small amounts of excess H_2O in order to determine 'fluid absent' melting is compensated by the advantage of producing small amounts of melts, even in regions where the hydrous phases are stable. These melts are buffered in all components and permit analysis of melt composition as a function of P and T. Additionally, the presence of melts enhances mineral growth (Fig. 3) and helps attain equilibrium. At higher amounts of partial melting the melt pools were large enough for analysis by microprobe and laser ablation-ICP-MS.

8. Trace element partitioning

Trace elements were measured in runs where the melt pools were large enough to be analyzed with a 23 μm diameter spot on the laser ablation-ICP-MS (Table 1) using Ca as the internal standard. Each time-resolved spectrum was carefully checked for possible contamination by trace element-rich phases. BSE images show that in large melt pools, small kyanite inclusions are often present (Fig. 3). However, kyanite does not contain detectable amounts of trace elements and Ca and therefore did not compromise the analyzed trace element composition of the melt. In order to visualize element enrichment or depletion in the melts, their compositions have been normalized to the starting material (Fig. 8a). In a second step, residue/melt partitioning has been calculated using the measured starting material/melt ratio and the estimated percentage of melt present in each experiment (Table 3). The partitioning behavior obtained provides first order constraints on trace element redistribution during partial melting of crustal material at high pressure (Fig. 8b).

The heavy rare earth elements (HREE) are all strongly compatible in the residue and reflect the high garnet/melt distribution coefficients of about 100–200. The bulk rock/melt partitioning at the mica melting curve is very similar over the investigated range, i.e. from 950°C, 3.0 GPa to

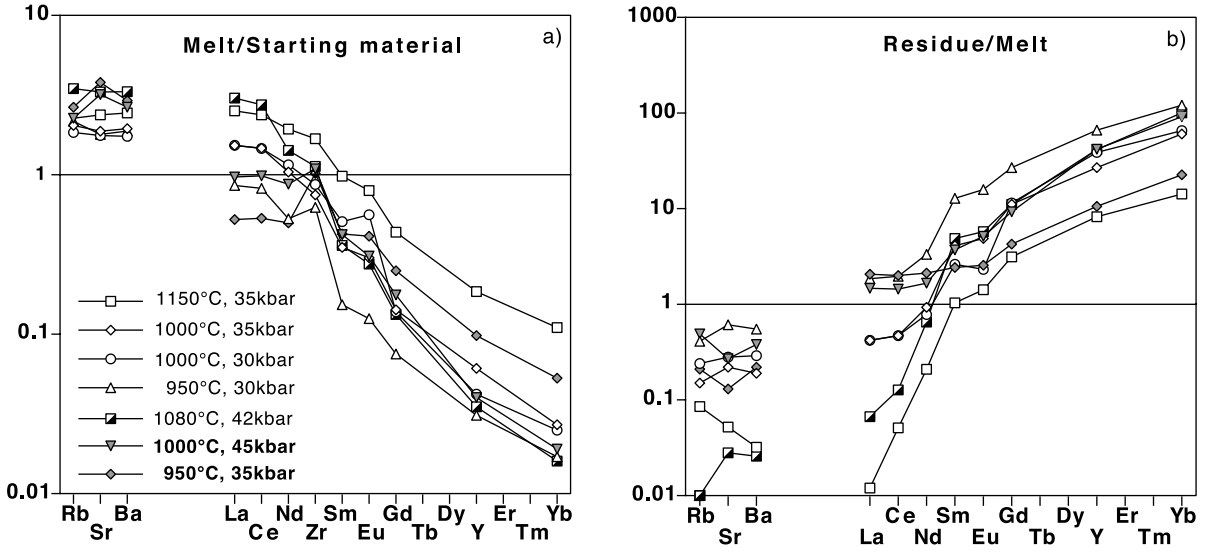

Fig. 8. (a) Trace element composition of melts normalized to the starting composition. Runs labeled in bold contain melt and phengite. (b) The residue/melt ratio is calculated from measured (starting material/melt) ratios and estimated amounts of melt in the runs (Table 1) using the equation $D(\text{residue/melt}) = \{D(\text{starting material/melt}) - X\}/\{1 - X\}$ with X = percentage of melt.

1080°C, 4.2 GPa. At significantly higher temperatures (1150°C, 3.5 GPa), the distribution coefficient of garnet/melt seems to decrease resulting in a less pronounced HREE enrichment in the high temperature residue (Fig. 8b). Rb, Sr and Ba (LILE) are incompatible and are enriched in the melt even if phengite is still stable (Fig. 8a) as in runs C-825 and UHP50. Microprobe analyses for Ba in phengite in run C-825 (950°C, 3.5 GPa) yield a phengite/melt partitioning of about 1.2. Given there is about 15 vol% of both melt and phengite in this run and phengite is the only significant solid sink for Ba, the whole rock/melt partitioning is of order 0.2, in agreement with the determined value (Fig. 8b). This example demonstrates that the Ba partitioning between whole rock and melt is strongly determined by the melt/mica ratio in the rock. The most surprising feature is the behavior of the light rare earth elements (LREE). In the high temperature runs with about 35–40% melt, the LREE are incompatible and display similar partitioning to Ba, Rb and Sr. Under the conditions of phengite melting, however, the LREE are compatible in the residue. This indicates the presence of a phase which strongly incorporates the LREE. In fact, in all these runs allanite has been observed (Fig. 3e). Allanite is an epidote group mineral that can incorporate LREE at percent levels. Accordingly minor amounts of allanite in the residue are able to change the LREE behavior from incompatible to compatible. A detailed study on the influence of allanite on REE distribution in subducted crust will be presented elsewhere.

9. Discussion

9.1. Stability of biotite and phengite

The experimental study demonstrates stability fields of biotite and phengite in crustal rock compositions such that these phases are able to transport H_2O and LILE to mantle depths. The presence of two hydrous phases complicates the phase relations and 'fluid absent' melting is not restricted to one single breakdown curve [24]. This study demonstrates that there is a KCMASH invariant point at about 950°C and 3.0 GPa, related to the melting of biotite and phengite (Fig. 7, right). At lower pressures, biotite melting (reaction 8) is at higher temperatures than phengite melting (reaction 7), which is consistent with observations in amphibolite to granulite facies terrains and low pressure experiments [22,23,25]. According to reaction 7, phengite melting produces biotite also and therefore the hydrous phases biotite and phengite are in a peritectic relationship during fluid absent melting as suggested by previous studies at lower pressures [22,23,25]. The subsolidus transition of biotite to phengite (reaction 4) conserves fluid, K and LILE which are then able to be retained at $P > 3.0$ GPa until melting of phengite through reaction 6. The reactant of this reaction is the assemblage Phe+Cpx+Cs, which is stable over a wide P–T range and over a large compositional range of subducted crustal rocks from K-MORB to pelitic sediments to granitic rocks [10–13]. Reaction 6 is therefore fundamental for phengite breakdown in all rock types of subducted crust at eclogite facies conditions.

The inferred region of phengite stability determined in this study extends $\sim$200°C higher than previously reported by Schmidt [15] in the system MORB+K_2O (curve 5 in Fig. 9). We suggest that the small amount of K_2O in the presence of small amounts of excess H_2O in the experiments of Schmidt [15] led to a complete solution of K_2O in the melt and thus to loss of phengite well before the fluid absent phengite melting curve was reached. In fact, recent experiments of Schmidt and Vielzeuf [26] with higher K_2O/H_2O ratios for K-MORB, greywacke and pelite with natural compositions, yield a very similar position for the phengite breakdown curve to that of the KCMASH system (curve 3 in Fig. 9). The change from the synthetic KCMASH system to the natural systems does not lead to a significant shift of reaction 6. This could be explained by opposite effects of Fe and Ti on reaction 6. Fe strongly partitions into and stabilizes garnet (shifting reaction 6 to lower T) whereas Ti stabilizes phengite (shifting reaction 6 to higher T) so that the net shift of reaction 6 is minor. The extension from KCMASH to Fe- and Ti-bearing systems is likely

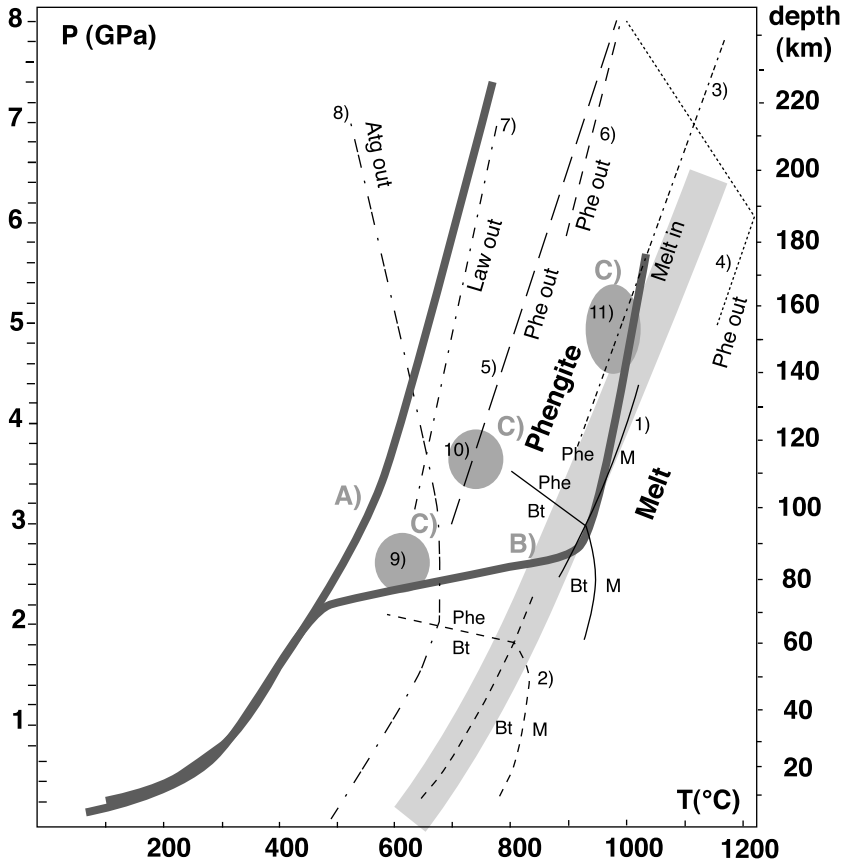

Fig. 9. Compiled *P–T* diagram with experimentally determined stability fields of phengite from different studies compared to calculated *P–T* loci from thermal modelling of subduction zones and *P–T* conditions of selected eclogite facies terrains. The gray band shows the best estimate for the position of phengite melting. (1) This study (see Fig. 7, right). (2) Biotite and phengite stability in metapelites in KFMASH [22]. (3) Location of main melt production in K-MORB, metapelite and metagreywacke [26]. (4) Titanian–phengite out-reaction in metapelite [17]. (5) Phengite out in K-MORB+small amounts of excess H_2O [15]. (6) Phengite out in a carbonate-bearing metapelite [29]. Major dehydration reactions in other slab materials: (7) Lawsonite (Law) stability in mafic rocks [31]. (8) Antigorite (Atg) stability in ultra-mafic rocks [30]. *P–T* data from exhumed ultra-high pressure terrains: (9) coesite–eclogite facies oceanic crust from Lago di Cignana, Western Alps [33]. (10) Coesite–eclogite facies continental crust from the Dora-Maira massif, Western Alps [12,49,50]. (11) Diamond facies gneisses from the Kokchetav massif, Kazakhstan [34]. *P–T* loci for top of subduction zones: (A) calculated for a 30° dip of the subduction surface and a velocity of 7.2 cm/yr [27]. A higher subduction angle would result in significantly lower temperatures for a given pressure. (B) Numerical model for subduction of a 25 Ma old lithosphere, subducting at 6 cm/yr and flattening at 80 km depth [37]. (C) *P–T* conditions of exhumed eclogites given in points (9)–(11) display higher temperatures than predicted by models like A).

to be much more important for the biotite to phengite transition (reaction 4) as with addition of Fe, the Opx field disappears and biotite+kyanite react to phengite+garnet. Vielzeuf and Holloway [22] proposed the occurrence of this transition at about 1.8 GPa for a bulk with Mg# = 0.5 (Fig. 9). Accordingly, the KCMASH system probably reflects a maximum pressure stability for biotite coexisting with kyanite and coesite. The influence of Na on phengite melting is likely to be of only minor importance because Na preferentially enters the clinopyroxene at high pressure (partitioning clinopyroxene/melt $\sim$1–3). Moreover, a single experiment (C-910; Table 2) in

NKCMASH at 3.5 GPa, 970°C contained phengite and melt indicating that the melting reaction was not shifted significantly due to the presence of Na.

With the addition of Na, Fe and Ti only rutile will form as an additional phase and therefore the univariant reaction 6 in KCMASH will turn into a tri-variant field in natural rocks. The melting of phengite will therefore occur over a temperature interval that is determined by the bulk rock composition. Clinopyroxene will be the first phase completely consumed in pelitic rocks whereas phengite is most likely the limiting phase for reaction 6 in a K-MORB composition.

9.2. Release of LILE during subduction

Fig. 9 shows a compilation of phengite stability in the *P–T* space. Phengite melting has a positive slope and occurs under conditions of about 800°C, 2.0 GPa up to at least 1000°C, 5.5 GPa. The upper pressure stability of phengite is not reached even at 8 GPa [15,16]. Generally, the published *P–T* loci calculated for the hot, uppermost part of a subducting oceanic crust of a mature subduction zone [27,28] are situated well within the stability field of phengite. Not even the addition of phengite-destabilizing components such as CO_2 [29] will reduce the phengite stability close to the calculated *P–T* loci. These observations constitute a dilemma given the well established enrichment of LILE in subduction zone magmas [1–3], which as a consequence can probably not be explained by a simple breakdown of the phase hosting these elements in deeply subducted crustal rocks. We propose three possible solutions to this dilemma.

9.2.1. Fluid fluxes partial melting

Partial breakdown of phengite may take place due to 'fluid present' instead of 'fluid absent' melting as suggested by Domanik and Holloway [16]. The source of such excess 'fluid' (or hydrous melt) could be dehydration of serpentine in the ultramafic layer [30] or of lawsonite in the mafic layer [31] of the subducted slab (see Fig. 9). The consumption of phengite is caused by the continuous reaction 2c during which the phengite content of the rock decreases and melt volume increases with increasing temperature for a fixed amount of available H_2O. Because of the inverted isotherms in subduction zones, temperature increases upwards in the top part of the subducted oceanic crust. Therefore, the melt volume produced by a certain amount of fluid in potassium-bearing rocks should increase with the upward movement of the melt. Such an increase in melt volume might enhance permeability and could help to efficiently remove partial melts from the slab. Trace element residue/melt partitioning (Fig. 8) demonstrates that significant amounts of LILE can be moved with the ascending melt even if phengite remains in the residuum. In such a scenario, the amount of consumed phengite is strongly dependent on the amount of H_2O available. The experiments revealed that the K content of buffered melts increases with temperature (Fig. 5d) while the H_2O content decreases (Tables 1 and 3). This finding suggests that the extraction of K becomes more efficient with increasing temperature, i.e. at greater depth of subduction for a constant position in the slab. It has to be evaluated if this increase in K content could be responsible for the observed increase in K content in subduction zone magmas with increasing depth [32].

If partial melting is triggered by fluids, it is likely, that trace element and isotopic signatures of the resulting hydrous melts are complex and inherit components of several rock types present in subducted crust. On the other hand, in H_2O-poor sections of the subducted slab phengite does not break down and some of the LILE are probably able to be transported to depths of at least 300 km [15,16].

9.2.2. Hot subduction

Some subduction zones may be hotter than conventional models predict, in which case 'fluid absent' phengite melting could be responsible for LILE release. Substantive evidence for higher thermal gradients in subduction zones comes from eclogite facies rocks. The deepest known subducted oceanic crust found today at the Earth's surface is represented by the coesite eclogites from Lago di Cignana, Western Alps, which underwent peak metamorphism at 600°C, 2.8

GPa [33]. They plot on much hotter *P–T* when compared to calculated values (Fig. 9). Even higher temperature for a given pressure is documented in ultra-high pressure metamorphosed continental crust (Fig. 9) of the Dora-Maira massif (Western Alps) and the Kokchetav massif (Kazaksthan). The latter is of potential significance because there exists evidence for partial melting during diamond facies, high pressure metamorphism [34–36]. This indicates that, at least in some subducted continental crust, phengite melting might be important for the release of LILE.

Recent thermal modelling has also demonstrated that slab melting could be caused by flat subduction [37]. The calculated *P–T* loci of Gutscher et al. [37] are at higher temperature than the determined stability of phengite and biotite in the interval of 2.8 –4.5 GPa (Fig. 9) and therefore significant amounts of LILE could be liberated during biotite and phengite melting at 80–150 km depth. In such a model, slab melting is not restricted to fast subduction of young oceanic crust with significant shear heating [28], and it follows that flat subduction may reconcile, at least partly, the discrepancy between calculated and reconstructed *P–T* loci. Partial melting of subducted mafic oceanic crust has been proposed for the origin of trondhjemite–tonalite–dacite (TTD) series [38]. Partial melting of sediments may contribute to the chemical signature of such rock suites. While major element composition of the experimentally determined partial melts have too low Al_2O_3 and too high K_2O contents compared to TTD, the trace element trends fit very well [39]. Especially the high Sr/Yb ratio of about 100 in the melts (Fig. 8a) indicates that partial melting of subducted sediments could contribute to the observed elevated LILE contents in TTD (e.g. [38]).

9.2.3. High pressure phengite breakdown

The LILE could be liberated when phengite breaks down to K-hollandite at depths of more than 300 km [15,29]. LILE partitioning between K-hollandite and phengite will need to be established in order to evaluate whether the LILE could be released efficiently by this phase transition.

9.3. Change in rock properties during partial melting of subducted crust

9.3.1. Chemical changes

Our results show that the extraction of granitic melt from crustal rock types leads to a fundamental change in the chemical character of the residue. For the investigated bulk composition and melt extraction of up to 30%, the silica content drops from 60 to 55 wt% (Fig. 5a). The residue is a kyanite–eclogite and contains the same minerals as an eclogite derived from mafic rocks. However, the amount of kyanite and probably the Fe/Mg ratio are much higher than in an eclogite derived from a mafic protolith. Reactions 2c or 6 lead to a significant redistribution of trace elements as demonstrated by the measured rock/melt partitioning (Fig. 8). Most of the LILE enter the melt while the HREE are retained in residual garnet. The LREE are buffered by the presence of accessory allanite and are not efficiently removed from this bulk composition at melt volumes below 30%. Allanite has been stabilized in the experiments by addition of 200–300 ppm of La and Ce and it is not a priori clear if allanite is present in subducted crust. However, allanite has been found as accessory phase in eclogite facies gneisses from China [40] and is present in eclogitic metagabbros [41], phengite eclogites and ultra-high pressure gneisses from the Western Alps [42]. This indicates that allanite is an important high pressure accessory mineral which probably influences the release of trace elements during partial melting. Hydrous melts extracted from subducted crust containing allanite are thus likely to be enriched in LILE but much less in LREE. This is consistent with observed chemical characteristics of subduction zone magmas, which have significantly higher LILE contents than MORB but do only show a moderate LREE enrichment [3,32]. The very low HREE content of the melts compared to LILE and LREE (Fig. 8a) suggests that the HREE characteristics of subduction zone magmas are not influenced by sediment melting, in agreement with geochemical studies of arc lavas [3]. Another characteristic of subduction zone magmas is their depletion in HFSE [1,3,32], which was not addressed in the present study. However,

previous experimental studies demonstrated that these elements strongly partition into rutile [43,44], which is expected to be a residual accessory phase in Ti-bearing, subducted crustal materials. Therefore, it is likely that residual rutile in subducted crust is at least partly responsible for the observed HFSE depletion [43,44].

This study proposes that silica-rich hydrous melts may contribute to the transfer of chemical tracers from subducted crust to subduction zone magmas. It must be considered that such a transfer is complex because these granitic melts probably react with the silica undersaturated mantle rocks and produce pyroxenes, garnet and phlogopite if the overlying mantle is at a similar temperature [45,46]. The stability and trace element partitioning of these phases modifies the trace element composition of the subduction-related component during later partial melting of the peridotite [7]. However, our experiments suggest that the estimated H_2O/K_2O ratio of the granitic melts extracted from the subducted crust is about 0.8–2 (see Tables 1 and 3) which is significantly greater than that of phlogopite ($\sim$0.45). Consequently, crystallizing phlogopite and/or pargasite in the mantle wedge are not able to store the entire H_2O content of the hydrous melt. If the temperature of the mantle wedge is above the thermal stability of the hydrous phases chlorite and serpentine there is no trap for such excess H_2O. It is therefore possible that a trace-element-rich fluid or hydrous melt may reach the locus of partial melting in the mantle wedge. In such a particular scenario, the chemical signature from slab components could be transferred to the subduction zone magmas via a hydrous melt or fluid. The chemical changes occurring during partial melting in subducted crust are not only important for the better understanding of arc-related magmatism but could influence within-plate magmatism because the residual kyanite–eclogite and the refertilized surrounding peridotite could participate in plume magmatism when recycled on a larger scale [47].

9.3.2. Physical changes

The removal of a K- and Si-rich granitic melt produces a kyanite- and garnet-rich residue. This transformation is coupled with a large increase in the density of the subducted rocks. Considering 30% of partial melting, the density of the investigated rock will change from about 3.15 to 3.4 g/cm^3 (i.e. from less dense to denser than the surrounding mantle rocks). If extensive fluid present melting occurs, the residue consists of kyanite and garnet only and such rocks would be the densest part of the down-going slab. Partial melting might also affect the rheology of subducted rocks. In the case of the deeply subducted, diamond facies gneisses from the Kokchetav massif, Hermann et al. [36] concluded that partial melting may have enhanced detachment of the rocks undergoing melting from the slab and that the melts might also have lubricated contacts during fast exhumation.

10. Conclusions

Phengite is the most important host for H_2O and LILE in potassium-bearing rocks at pressures above 2 GPa. The observed reaction: Phe+Cpx+Cs $\pm$ fluid $\rightarrow$ Grt+Ky+Melt $\pm$ Kfs is fundamental for melting of subducted crust because phengite, coesite and clinopyroxene are present in nearly all crustal rock types at high pressure. Phengite breakdown in hot or flat subduction zones might be responsible for the liberation of LILE and H_2O, which are generally enriched in subduction zone magmas. However, the stability of phengite to high temperature and pressure prevents LILE release in subduction zones with a typically 'cold' thermal gradient. We suggest that, in such a tectonic setting, fluids originating from the dehydration of subducted mafic and ultra-mafic rocks most probably react with phengite-bearing rocks in order to produce hydrous granitic melts, which then transfer H_2O and LILE from the slab to the mantle wedge. Trace element and isotopic signatures of such melts are likely to be complex and they should inherit signals from all the different rock types involved. The observed increase of K_2O and decrease of H_2O content in the melt with increasing temperature suggests that the extraction of K is more efficient at greater depths of subduction. As the

H_2O/K_2O ratio of hydrous granitic melts is significantly higher than that of phlogopite, it is unlikely that the entire granitic melt reacts and crystallizes when it comes into contact with peridotites from the mantle wedge. Consequently it is possible that at least some of the released H_2O and trace element inventory from the subducted crust may reach the locus of subduction zone magma genesis.

Acknowledgements

We would like to thank W.O. Hibberson and D. Scott for technical assistance in the high pressure laboratory, F. Brink, D. Vowles and S. Stowe from the Electron Microscope Unit (ANU) and N. Ware from RSES for their help with mineral analyses and C. Allen for assistance in conducting the ICP-MS analyses. This work benefited from fruitful discussions with S. Eggins, G. Yaxley and H. O'Neill. Comments by D. Rubatto and S. Eggins and constructive reviews by S. Harley, P. Ulmer and an anonymous reviewer helped to improve the manuscript. J.H. acknowledges the financial support of the Schweizerischer Nationalfonds ('Nachwuchsstipendium') and the Australian Research Council. *[AH]*

References

[1] M.R. Perfit, D.A. Gust, A.E. Bence, R.J. Arculus, S.R. Taylor, Chemical characteristics of island-arc basalts: implications for mantle sources, Chem. Geol. 30 (1980) 227–256.

[2] R.W. Kay, Volcanic arc magmas: implications of a melting–mixing model for element recycling in the crust-upper mantle system, J. Geol. 88 (1980) 497–522.

[3] M.T. McCulloch, J.A. Gamble, Geochemical and geodynamical constraints on subduction zone magmatism, Earth Planet. Sci. Lett. 102 (1991) 358–374.

[4] T. Plank, C.E. Langmuir, Tracing trace elements from sediment input to volcanic output at subduction zones, Nature 362 (1993) 739–743.

[5] P. Schiano, N. Clocchiatti, N. Shimizu, R.C. Maury, K.P. Jochum, A.W. Hoffman, Hydrous, silica-rich melts in the sub-arc mantle and their relationship with erupted arc magmas, Nature 377 (1995) 595–600.

[6] Y. Tatsumi, M. Murasaki, E.M. Arsadi, S. Nohda, Geochemistry of Quarternary lavas from NE Sulawesi: transfer of subduction components into the mantle wedge, Contrib. Mineral. Petrol. 107 (1991) 137–149.

[7] Y. Tatsumi, T. Kogiso, Trace element transport during dehydration processes in the subducted oceanic crust: 2. Origin of chemical and physical characteristics in arc magmatism, Earth Planet. Sci. Lett. 148 (1997) 207–221.

[8] H. Bureau, H. Keppler, Complete miscibility between silicate melts and hydrous fluids in the upper mantle: experimental evidence and geochemical implications, Earth Planet. Sci. Lett. 165 (1999) 187–196.

[9] R. Stalder, P. Ulmer, A.B. Thompson, D. Günther, Experimental approach to constrain second critical end points in fluid/silicate systems: near-solidus fluids and melts in the system albite–H_2O, Am. Mineral. 85 (2000) 68–77.

[10] S.S. Sorenson, J.N. Grossman, M.R. Perfit, Phengite-hosted LILE enrichment in eclogite and related rocks implications for fluid-mediated mass transfer in subduction zones and arc magma genesis, J. Petrol. 38 (1997) 3–34.

[11] D.A. Carswell, P.J. O'Brien, R.N. Wilson, M. Zhai, Thermobarometry of phengite-bearing eclogites in the Dabie Mountains of central China, J. Metamorph. Geol. 15 (1997) 239–252.

[12] R. Compagnoni, T. Hirajima, C. Chopin, Ultra-high-pressure metamorphic rocks in the Western Alps, in: R.G. Coleman, X. Wang (Eds.), Ultrahigh Pressure Metamorphism, Cambridge University Press, Cambridge, 1995, pp. 206–243.

[13] C. Meyre, C. De Capitani, T. Zack, M. Frey, Petrology of high-pressure metapelites from the Adula Nappe (Central Alps, Switzerland), J. Petrol. 40 (1999) 199–213.

[14] K.J. Domanik, R.L. Hervig, S.M. Peacock, Beryllium and boron in subduction zone minerals: an ion microprobe study, Geochim. Cosmochim. Acta 57 (1993) 4997–5010.

[15] M.W. Schmidt, Experimental constraints on recycling of potassium from subducted oceanic crust, Science 272 (1996) 1927–1930.

[16] K.J. Domanik, J.R. Holloway, The stability of phengitic muscovite and associated phases from 5.5 to 11 GPa: implications for deeply subducted sediments, Geochim. Cosmochim. Acta 60 (1996) 4133–4150.

[17] S. Ono, Stability limits of hydrous minerals in sediment and mid-ocean ridge basalt compositions: implications for water transport in subduction zones, J. Geophys. Res. 103 (1998) 18253–18267.

[18] W.C. Luth, O. Ingamells, Gel preparation of starting materials for hydrothermal experimentation, Am. Mineral. 50 (1965) 255–258.

[19] S.M. Eggins, R.L. Rudnick, W.F. McDonough, The composition of peridotites and their minerals: a laser ablation ICP-MS study, Earth Planet. Sci. Lett. 154 (1998) 53–71.

[20] R.G. Berman, Internally consistent thermodynamic data for minerals in the system Na_2O–K_2O–CaO–MgO–Fe_2O_3–Al_2O_3–SiO_2–TiO_2–H_2O–CO_2, J. Petrol. 29 (1988) 445–522.

[21] H.J. Massone, Z. Szpurzka, Thermodynamic properties of white micas on the basis of high-pressure experiments in

the systems K_2O–MgO–Al_2O_3–SiO_2–H_2O and K_2O–FeO–Al_2O_3–SiO_2–H_2O, Lithos 41 (1997) 229–250.
[22] D. Vielzeuf, J.R. Holloway, Experimental determination of the fluid-absent melting relations in the pelitic system, Contrib. Mineral. Petrol. 98 (1988) 257–276.
[23] N. Le Breton, A.B. Thompson, Fluid-absent dehydration melting of biotite in metapeliotes in the early stage of crustal anatexis, Contrib. Mineral. Petrol. 99 (1988) 226–237.
[24] D. Vielzeuf, Melting phase relations in hydrous systems revisited, J. Conf. 5 (2000) 106.
[25] A.E. PatiñoDouce, N. Harris, Experimental constraints on Himalayan anatexis, J. Petrol. 39 (1998) 689–710.
[26] M.W. Schmidt, D. Vielzeuf, Differential melt productivity of MORB, greywacke and pelite during subduction, J. Conf. 5 (2000) 92–93.
[27] J.H. Davies, D.J. Stevenson, Physical model of source region of subduction zone volcanics, J. Geophys. Res. 97 (1992) 2037–2070.
[28] S.M. Peacock, T. Rushmer, A.B. Thompson, Partial melting of subducted oceanic crust, Earth Planet. Sci. Lett. 121 (1994) 227–244.
[29] K.J. Domanik, J.R. Holloway, Experimental synthesis and phase relations of phengitic muscovite from 6.5 to 11 GPa in a calcareous metapelite from the Dabie Mountains, China, Lithos 52 (2000) 51–77.
[30] P. Ulmer, V. Trommsdorff, Serpentine stability to mantle depths and subduction-related magmatism, Science 268 (1995) 858–861.
[31] S. Poli, M.W. Schmidt, H_2O transport and release in subduction zones: experimental constraints on basaltic and andesitic systems, J. Geophys. Res. 100 (1995) 22299–23314.
[32] Y. Tatsumi, S.M. Eggins, Subduction Zone Magmatism, Blackwell, Cambridge, 1995.
[33] T. Reinecke, Very-high-pressure metamorphism and uplift of coesite-bearing metasediments from the Zermatt-Saas zone, Western Alps, Eur. J. Mineral. 3 (1991) 7–17.
[34] V.S. Shatsky, N.V. Sobolev, M.A. Vavilov, Diamond-bearing metamorphic rocks of the Kokchetav Massif (Northern Kazakhstan), in: R.G. Coleman, X. Wang (Eds.), Ultrahigh Pressure Metamorphism, Cambridge University Press, Cambridge, 1995, pp. 427–455.
[35] V.S. Shatsky, E. Jagoutz, N.V. Sobolev, O.A. Kozmenko, V.S. Parkhomenko, M. Troesch, Geochemistry and age of ultrahigh pressure metamorphic rocks from the Kokchetav massif (Northern Kazakhstan), Contrib. Mineral. Petrol. 137 (1999) 185–205.
[36] J. Hermann, D. Rubatto, A. Korsakov, V.S. Shatsky, Age and exhumation rate of diamondiferous, deeply subducted continental crust in the Kokchetav massif, Kazakhstan, Contrib. Mineral. Petrol. (2001), in press.
[37] M.A. Gutscher, R. Maury, J.P. Eissen, B. Erwan, Can slab melting be caused by flat subduction?, Geology 28 (2000) 535–538.
[38] M.J. Defant, M.S. Drummond, Derivation of some modern arc magmas by melting young subducted lithosphere, Nature 347 (1990) 662–665.
[39] M.S. Drummond, M.J. Defant, A model for trondhjemite–tonalite–dacite genesis and crustal growth via slab melting: archean to modern comparisons, J. Geophys. Res. 95 (1990) 21503–21521.
[40] D.A. Carswell, R.N. Wilson, M. Zhai, Metamorphic evolution, mineral chemistry and thermobarometry of schists and orthogneisses hosting ultra-high pressure eclogites in the Dabieshan of central China, Lithos 52 (2000) 121–155.
[41] R. Tribuzio, B. Messiga, R. Vannucci, P. Bottazzi, Rare earth element redistribution during high-pressure low-temperature metamorphism in ophiolitic Fe–gabbros (Liguria, northwestern Italy): implications for light REE mobility in subduction zones, Geology 24 (1996) 711–714.
[42] J. Hermann, Stability of allanite to high pressure-temperature: implications for light rare-earth-element budget in subducted crust, LPI Contrib. 971 (1999) 122–123.
[43] R. Stalder, S.F. Foley, G.P. Brey, I. Horn, Mineral-aqueous fluid partitioning of trace elements at 900–1200°C and 3.0–5.7 GPa: new experimental data for garnet, clinopyroxene and rutile and implications for mantle metasomatism, Geochim. Cosmochim. Acta 62 (1998) 1781–1801.
[44] J.M. Brenan, H.F. Shaw, F.J. Ryerson, D.L. Phinney, Rutile-fluid partitioning of Nb, Ta, Zr, U and Th: implications for high-field-strength element depletion in island-arc basalts, Earth Planet. Sci. Lett. 128 (1994) 327–339.
[45] J. Konzett, P. Ulmer, The stability of hydrous potassic phases in lherzolitic mantle: an experimental study to 9.5 GPa in simplified and natural bulk compositions, J. Petrol. 40 (1999) 629–652.
[46] G.M. Yaxley, D.H. Green, Reactions between eclogite and peridotite: mantle refertilisation by subduction of oceanic crust, Schweiz. Mineral. Petrogr. Mitt. 78 (1998) 243–255.
[47] G. Yaxley, Experimental study of the phase and melting relations of homogeneous basalt+peridotite mixtures and implications for the petrogenesis of flood basalts, Contrib. Mineral. Petrol. 139 (2000) 326–338.
[48] P.W. Mirwald, H.J. Massone, The low–high quartz and quartz–coesite transition to 40 kbar between 600°C and 1600°C and some reconnaissance data on the effect of $NaAlO_2$ component on the low quartz–coesite transition, J. Geophys. Res. 85 (1980) 6983–6990.
[49] C. Chopin, C. Henry, A. Michard, Geology and petrology of the coesite-bearing terrain, Dora Maira massif, Western Alps, Eur. J. Mineral. 3 (1991) 263–291.
[50] H.-P. Schertl, W. Schreyer, C. Chopin, The pyrope–coesite rocks and their country-rocks at Parigi, Dora Maira Massif, Western Alps: detailed petrography, mineral chemistry and *PT* path, Contrib. Mineral. Petrol. 108 (1991) 1–21.